NASA Contractor Report 162752

NASA-CR-162752
19800009164

MINIATURE PIEZORESISTIVE SOLID STATE INTEGRATED PRESSURE SENSORS

Seun K. Kahng

UNIVERSITY OF OKLAHOMA
Norman, Oklahoma 73019

NASA Grant NSG-1481
February 1980

National Aeronautics and
Space Administration

Langley Research Center
Hampton, Virginia 23665

NF02043

Final Report

on

MINIATURE PIEZORESISTIVE SOLID STATE INTEGRATED PRESSURE SENSORS

Grant NSG-1481

Submitted to

NATIONAL AERONAUTICS AND SPACE ADMINISTRATION

Prepared by

Seun K. Kahng

Professor of Electrical Engineering and Computing Sciences
University of Oklahoma

Submitted by

Office of Research Administration

University of Oklahoma

Norman, Oklahoma

73019

February 1980

TABLE OF CONTENTS

ABSTRACT

The characteristics of silicon pressure sensors with an ultra-small diaphragm are described. The pressure sensors utilize rectangular diaphragms as small as 0.0127 x 0.0254 cm and a p-type Wheatstone bridge consisting of diffused piezoresistive elements, 0.000254 cm by 0.00254 cm. These sensors exhibit as high as 0.5 MHz natural frequency and 1 mV/V/psi pressure sensitivity. Fabrication techniques and high frequency results from shock tube testing and low frequency (< 60 KHz) comparison with microphones are presented.

A MINIATURE HIGH FREQUENCY SILICON PRESSURE SENSOR

INTRODUCTION

Piezoresistive silicon pressure sensors have gained considerable recognition in the application of dynamic pressure measurements in various areas such as aerodynamics, process control, and others. Recently, there has been an increased demand for a miniature pressure transducer which exhibits high sensitivity and high natural frequency. The primary investigative fields requiring this type of pressure sensor are boundary layer, jet noise, and noise abatement research. With a transducer having near 1 MHz first mode natural frequency, a much needed harmonic analysis of the pressure can be accomplished.

The purpose of this work was to exploit upper limit frequency of a miniature pressure sensor with an acceptable sensitivity. The upper limit frequency and sensitivity to achieve were set at ½ MHz and 1 mv/v/psi (1.451×10^{-4} mv/v-N/m^2), respectively.

Since Smith's [1] studies of the piezoresistance effect in silicon, a number of different devices have incorporated this effect into their design for purposes of measurement of dynamic pressure. This is due not only to the large magnitude of this effect in silicon, but also because of the advanced state of silicon integrated circuits fabrication technology. The demand for a smaller and higher frequency pressure transducer necessitated the use of a thin diaphragm which amplifies the stresses due to applied pressure.

Interests in biomedical applications of a miniature solid state pressure transducer led to the development of a silicon pressure sensor small and sensitive enough to be implanted in the human body for blood pressure analysis [2]. With some design modifications of a sensor of this type a ½ MHz first mode natural frequency pressure transducer can be

fabricated.

Though sensors can be made extremely small as VLSI technology becomes available, it is intended in this work to use conventional silicon device technology which is readily available to many industries and universities.

The transducers were fabricated on n-type (100) orientation silicon wafers using standard integrated circuit processing techniques. Testing of the transducers, some of which was done at NASA-Langley in Virginia, included evaluation of the sensor's first mode natural frequency and frequency response.

The emphasis of the work done is toward the design and fabrication of a high frequency silicon pressure sensor. A silicon pressure sensor with a natural frequency at 625 KHz and sensitivity of 0.82 mv/v-psi (1.2×10^{-4} mv/v-N/m^3) has been accomplished with a rectangular diaphragm dimensions of 1.27×10^{-2} cm x 2.54×10^{-2} cm x 1.06 μm.

THEORETICAL AND DESIGN CONSIDERATIONS

For an arbitrarily oriented diffused resistive strip, the following equation relates the fractional change in resistivity to the applied stresses at a given point,

$$\frac{\Delta\rho}{\rho_o} = \pi_\ell\sigma_\ell + \pi_t\sigma_t + \pi_t'\sigma_t' \tag{1}$$

where

$$\pi_\ell = \pi_{11} - 2(\pi_{11} - \pi_{12} - \pi_{44})(\ell_1^2m_1^2 + \ell_1^2n_1^2 + m_1^2n_1^2)$$

and

$$\pi_t = \pi_{12} + (\pi_{11} - \pi_{12} - \pi_{44})(\ell_1^2\ell_2^2 + m_1^2m_2^2 + n_1^2n_2^2)$$

In the expressions, σ_ℓ is the longitudinal component of stress applied to the sample, σ_t one component of the transverse stress, ℓ_1, m_1, n_1 the direction cosines between the longitudinal direction of the sample and the cubic axes, and ℓ_2, m_2, n_2 the direction cosines between the direction of one component of the transverse stress and the cubic axes. The longitudinal direction is taken to be parallel to the applied electric field. The π_t' and σ_t' refer to a possible second component of the transverse stress. For our purposes, this second component of transverse stress will act in a direction perpendicular to the surface of the diaphragm. This component will be neglected since it is several orders of magnitude smaller than the other two components of stress, σ_ℓ and σ_t.

Since Eq. (1) is a point relation, the stress must be averaged over the area of a finite dimension of resistor strip. Neglecting the second component of transverse stress, σ_t', the diffused strip will have a piezoresistance effect given by,

$$\left(\frac{\Delta R}{R_o}\right) = \pi_\ell\bar{\sigma}_\ell + \pi_t\bar{\sigma}_t \tag{2}$$

Where $\bar{\sigma}_\ell$ and $\bar{\sigma}_t$ are the average stresses on the diaphragm along the longitudinal and transverse directions, of the strip, respectively. Equation (2) reduces to the following relation for a p-type diffused resistor.

$$\frac{\Delta R}{R_o} \simeq \frac{\pi_{44}}{2} \bar{\sigma}_\ell - \frac{\pi_{44}}{2} \bar{\sigma}_t \simeq \frac{\pi_{44}}{2} (\overline{\sigma_\ell - \sigma_t}) \qquad (3)$$

$(\overline{\sigma_\ell - \sigma_t})$ denotes the averaged value for the difference in the longitudinal and transverse stress across the entire area of the resistor.

The distribution of the stress-difference, $(\sigma_x - \sigma_y)$, on the diaphragm depends on its length and width, a and b, Fig. 1.

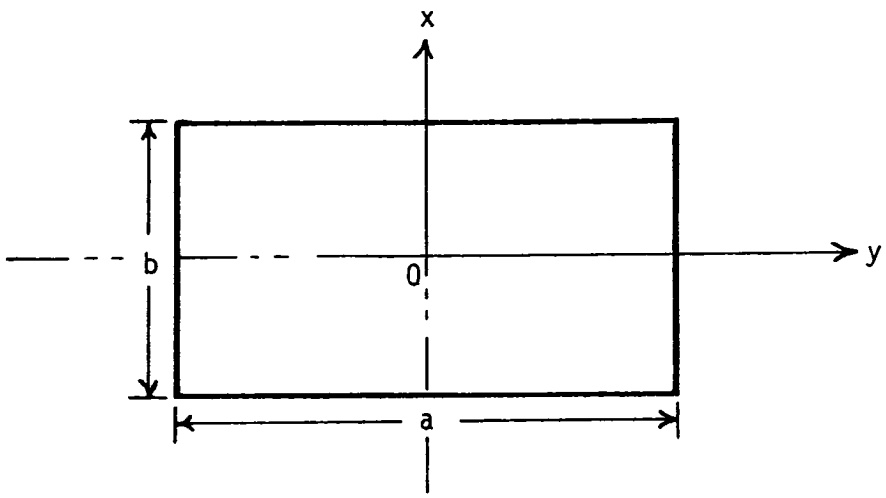

Figure 1. Diaphragm's Reference Coordinate System

Figure (2) is the sketch of the entire pressure transducer after processing and dicing into single chips. The thickness of the diaphragm determines the magnitude of $(\sigma_x - \sigma_y)$ at each point. Generally, the larger and thinner the diaphragm is made, for a set ratio of a/b, the higher the magnitude of the stresses will be for a given amount of pressure applied uniformly to the diaphragm's surface.

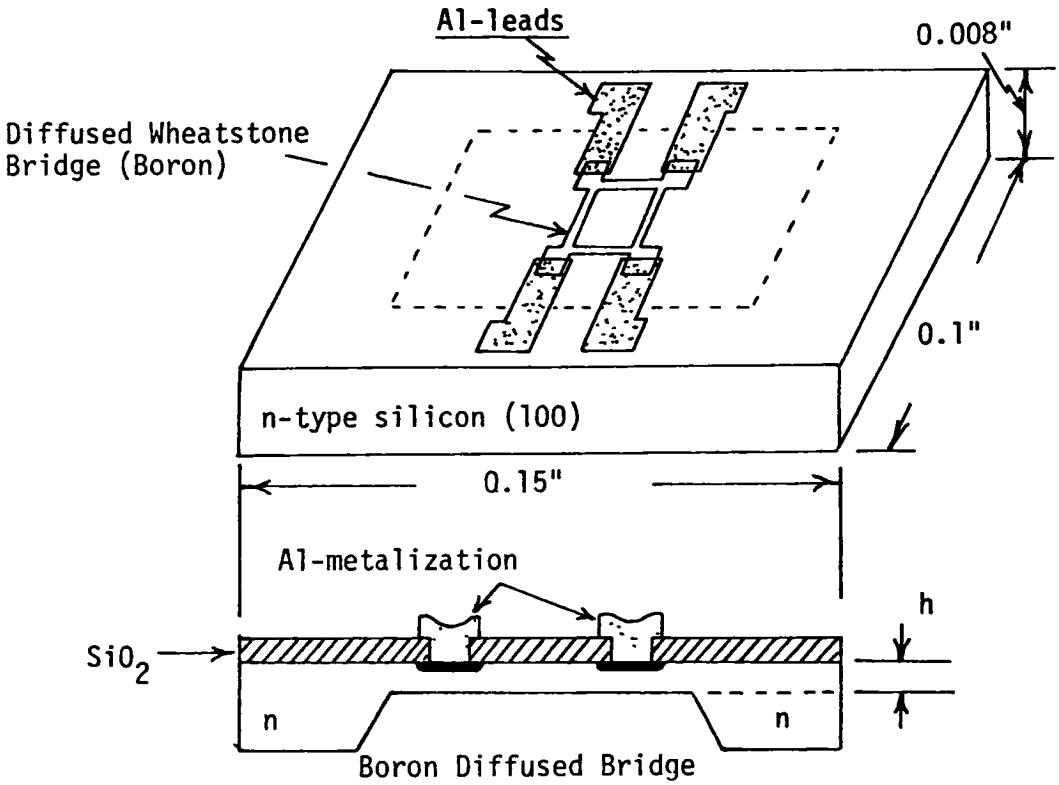

Figure 2. Boron Diffused Silicon Pressure Sensor (h = thickness)

For a rectangular plate, Warburton [3] approximates the natural frequency by applying the Rayleigh method (Rayleigh 1894, p. 109 et seq.) and by assuming that the waveforms of vibrating plates and beams are similar. The approximation for the first mode natural frequency is

$$f_n = \frac{\lambda h \pi}{a^2} \left[\frac{Eg}{48\rho(1 - \nu^2)} \right]^{\frac{1}{2}} \tag{4}$$

where

λ = non-dimensional frequency factor

h = diaphragm thickness

E = Young's Modulus

ρ = weight per unit volume

g = acceleration due to gravity

ν = Poisson's ratio

a = length of diaphragm

b = width of diaphragm

The non-dimensional frequency factor, λ, is derived from the relation,

$$\lambda^2 = G_x^4 + G_y^4 \frac{a^4}{b^2} + \frac{2a^2}{b^2} [\nu H_x H_y + (1 - \nu) J_x J_y] \tag{5}$$

where the coefficients G_x, G_y, H_x, H_y, J_x, and J_y depend on the nodal pattern and the boundary conditions. For a plate with all four edges clamped and 2 nodal lines, corresponding to the edges, in both the x and the y directions, these coefficients become,

$$G_x = G_y = 1.506 \qquad H_x = H_y = J_x = J_y = 1.248$$

Substituting these values into Eq. (8) gives,

$$\lambda^2 = (1.506)^4 (1 + \frac{a^4}{b^4}) + \frac{a^2}{b^2} 2(1.248)^2 \tag{6}$$

thus,

$\lambda = 3.66$ for a/b = 1

and

$\lambda = 10.00$ for a/b = 2

Using the following values, typical for silicon, and the appropriate conversion constants to substitute into Eq. (4),

$E \simeq 1.5 \times 10^{12}$ gm/cm sec^2

$\rho \simeq [2.328$ gms/$cm^3]g$

$\nu \simeq .3$

gives the following relationship between the diaphragms first mode natural frequency and its length, width and thickness.

$$f_n = 2.154 \times 10^5 \frac{h}{a^2} \qquad \text{for } a/b = 1 \tag{7-a}$$

and

$$f_n = 5.906 \times 10^5 \frac{h}{a^2} \qquad \text{for } a/b = 2 \tag{7-b}$$

where h and a are given in centimeters, and f_n in Hz.

In order to increase the first mode natural frequency of a diaphragm, the diaphragm's dimensions can be reduced or the thickness of the diaphragm can be increased. Both of these alternatives will lower the magnitude of the stresses on the diaphragm which in turn lowers the sensitivity of the transducer. By choosing a desired first mode natural frequency it is possible to calculate the sensitivity for different dimensions of the diaphragm. For sensitivity calculations, the diaphragm thickness can be calculated given the diaphragm dimensions and the desired first mode frequency using Eq. (4). The thickness is then given by

$$h = \frac{a^2 f_n}{\lambda \pi} \left[\frac{Eg}{48(1 - \nu^2)}\right]^{-\frac{1}{2}} \tag{8}$$

Calculations made by computer analyses of the stress distribution on a square diaphragm are given in Table I. The values given are the difference between the x and y components of stress $(\sigma_x - \sigma_y)$ at points along a line from the center of the diaphragm (x = 0, y = 0) to the middle of the edge (x = b/2, y = 0) for different diaphragm sizes, see Fig. 3. q is defined as pressure input in psi. The values of the stress difference along the y axis from (0,0) to (0,a/2) will be the same values given in Table I with opposite signs.

Tables II-a and II-b give the values of $(\sigma_x - \sigma_y)$ for a rectangular diaphragm, a/b2 = 2, at points along the x axis from (0,0) to (b/2,0) and at points along the y axis from (0,0) to (0,a/2), respectively.

The data in these three tables indicate that for a given first mode

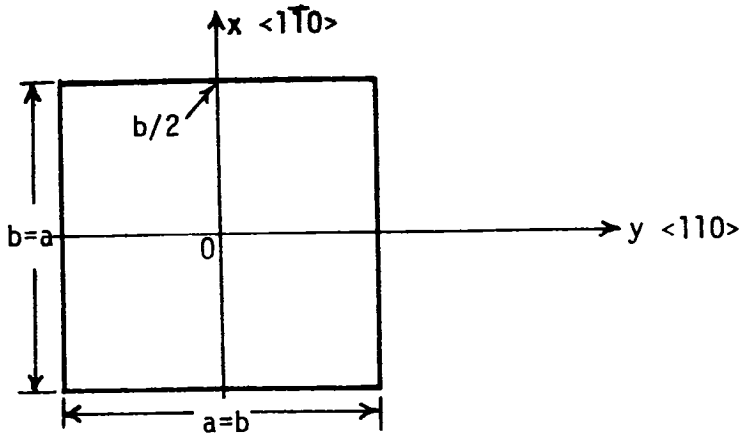

Figure 3. Square Diaphragm Coordinate System.

frequency, a reduction in diaphragm dimensions along with the corresponding decrease in the diaphragm's thickness will increase the magnitude of the stress difference ($\sigma_x - \sigma_y$) at each point. With proper positioning of a resistor to areas of high stress, the change in resistance can be increased by decreasing the dimensions of the diaphragm. The amount by which the dimensions may be decreased will of course be limited due to alignment problems which might arise in the photolithographic process used in etching patterns on the diaphragm.

The stress pattern on the diaphragm varies in shape as well as magnitude as the ratio of length to width increases from unity. On a square diaphragm, the value of ($\sigma_x - \sigma_y$) is zero at the center and along the lines $x = \pm y$, Fig. 4. The stress difference's magnitude is appreciable only in the vicinity of the middle of the edges.

The stress distribution along the y axis for ($\sigma_x - \sigma_y$) will be just the negative of the x axis distribution shown in Fig. 3. To locate a resistor in an area of high stress, it would have to be positioned very close to the edge of the diaphragm. This could cause problems in alignment due to the narrowness of the high stress region.

Table I $(\sigma_x - \sigma_y)/q$ for 1 MHz First Mode Natural Frequency.

a=b [mil]	h μm \ X	0	$\frac{2b}{20}$	$\frac{4b}{20}$	$\frac{6b}{20}$	$\frac{8b}{20}$	$\frac{b}{2}$
5	1.16	0	-1.640	41.79	282.4	996.3	2608.0
7	2.27	0	-0.835	21.32	144.1	508.3	1331.0
9	3.74	0	-0.504	12.90	087.2	307.5	0805.0
11	5.59	0	-0.340	08.60	058.4	205.8	0539.0
13	7.81	0	-0.240	06.20	041.8	147.4	0385.8
15	10.40	0	-0.180	04.60	031.4	110.7	0290.0
17	13.40	0	-0.140	03.60	024.4	086.2	0225.6
19	16.70	0	-0.110	02.90	019.6	069.0	0181.0
21	20.40	0	-0.090	02.40	016.0	056.5	0148.0
23	24.50	0	-0.080	02.00	013.4	047.1	0123.3
25	28.90	0	-0.070	01.70	011.3	039.9	0104.3

a=2b bxa mil	h μm \ X	0	$\frac{b}{10}$	$\frac{2b}{10}$	$\frac{3b}{10}$	$\frac{4b}{10}$	$\frac{b}{2}$
5 x 10	1.69μ	-849.	-748.	-438.	99.	890.	1962.
7 x 14	3.32	-433.	-382.	-224.	50.	454.	1001.
9 x 18	5.49	-262.	-231.	-135.	31.	275.	0606.
11 x 22	8.20	-175.	-155.	-091.	20.	184.	0405.
13 x 26	11.50	-126.	-110.	-065.	15.	132.	0290.
15 x 30	15.25	-094.	-083.	-049.	11.	099.	0218.
17 x 34	19.60	-073.	-065.	-038.	09.	077.	0170.
19 x 38	24.5	-059.	-052.	-030.	07.	062.	0136.
21 x 42	29.9	-048.	-042.	-025.	06.	050.	0111.
23 x 46	35.8	-040.	-035.	-021.	05.	042.	0093.
25 x 50	42.4	-034.	-030.	-018.	04.	036.	0078.

Table II-a. $(\sigma_x - \sigma_y)/q$ for 1 MHz First Mode Natural Frequency.

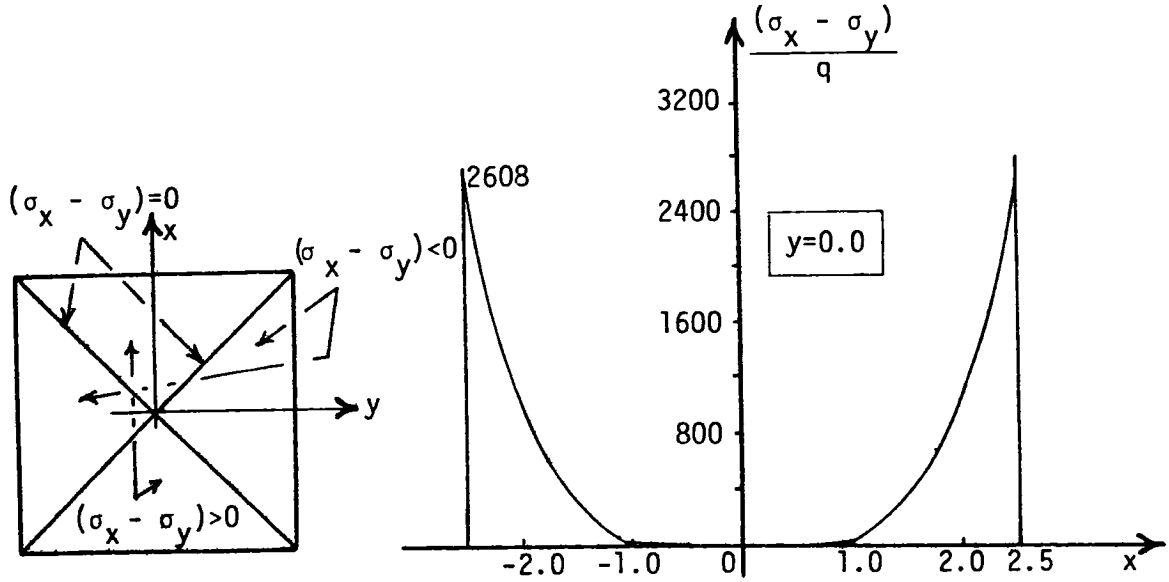

Figure 4. Stress Distribution for 5 mil x 5 mil x 1.16 μm (1.27×10^{-2} cm x 1.27×10^{-2} cm x 1.16 μm) Diaphragm

Table II-b. $\frac{(\sigma_x - \sigma_y)}{q}$ for 1 MHz First Mode Natural Frequency

b/a = 2 bxa [mils]	Y h [μm]	0	$\frac{2a}{10}$	$\frac{2a}{10}$	$\frac{3a}{10}$	$\frac{4a}{10}$	$\frac{a}{2}$
5 x 10	1.69	-849.	-788.	-603.	-344.	-289.	-1345.
7 x 14	3.32	-433.	-402.	-308.	-175	-148.	-0686.
9 x 18	5.49	-262.	-243.	-186	-106.	-892	-0415.
11 x 22	8.20	-175.	-163.	-125.	-071.	-060.	-0278.
13 x 26	11.50	-126.	-117.	-089.	-051.	-043.	-0199.
15 x 30	15.25	-094.	-088.	-067.	-038.	-032.	-0149
17 x 34	19.60	-073.	-068.	-052.	-030.	-025.	-0116.
19 x 38	24.50	-059.	-055.	-042.	-024.	-020.	-0093.
21 x 42	29.90	-048.	-045.	-034.	-019.	-016.	-0076.
23 x 46	35.80	-040.	-037.	-029.	-016.	-014	-0064.
25 x 50	42.40	-034.	-032.	-024.	-014.	-012.	-0054.

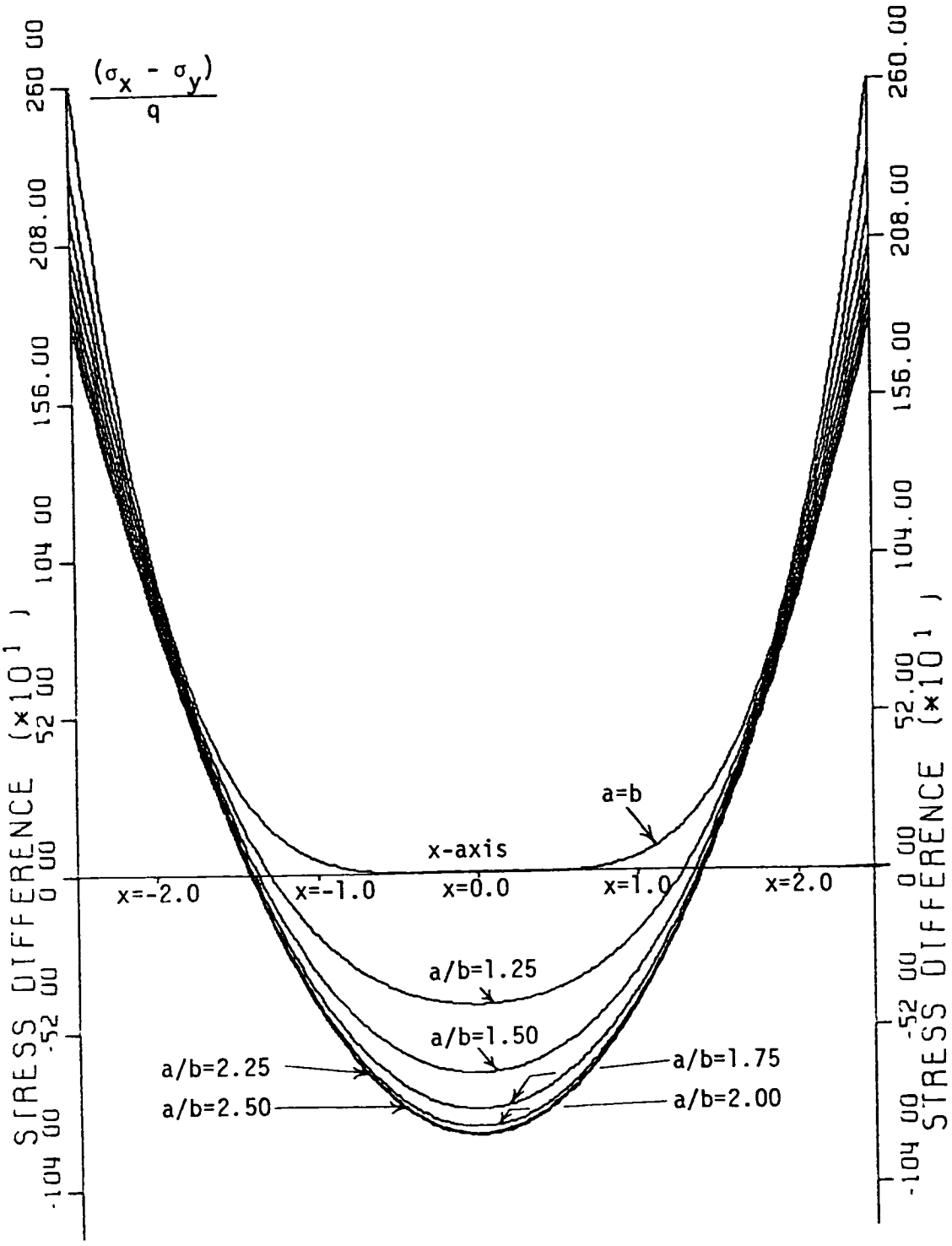

Figure 5. Stress Distribution Along x-axis for Various Ratios, a/b, b=5.0 mil

However, as the ratio a/b increases from unity, the magnitude of the stress difference, $|\sigma_x - \sigma_y|$, increases at the center of the diaphragm, Fig. 5. At a/b = 2, this center region has a relatively high magnitude of $|\sigma_x - \sigma_y|$ over a larger area than the narrower regions toward the edge of the diaphragm. Fig. 6 shows the value of $(\sigma_x - \sigma_y)$ along lines parallel to the x axis at different values of y. The stresses were calculated for a 5 x 10 mil diaphragm designed for 1 MHz first-mode natural frequency.

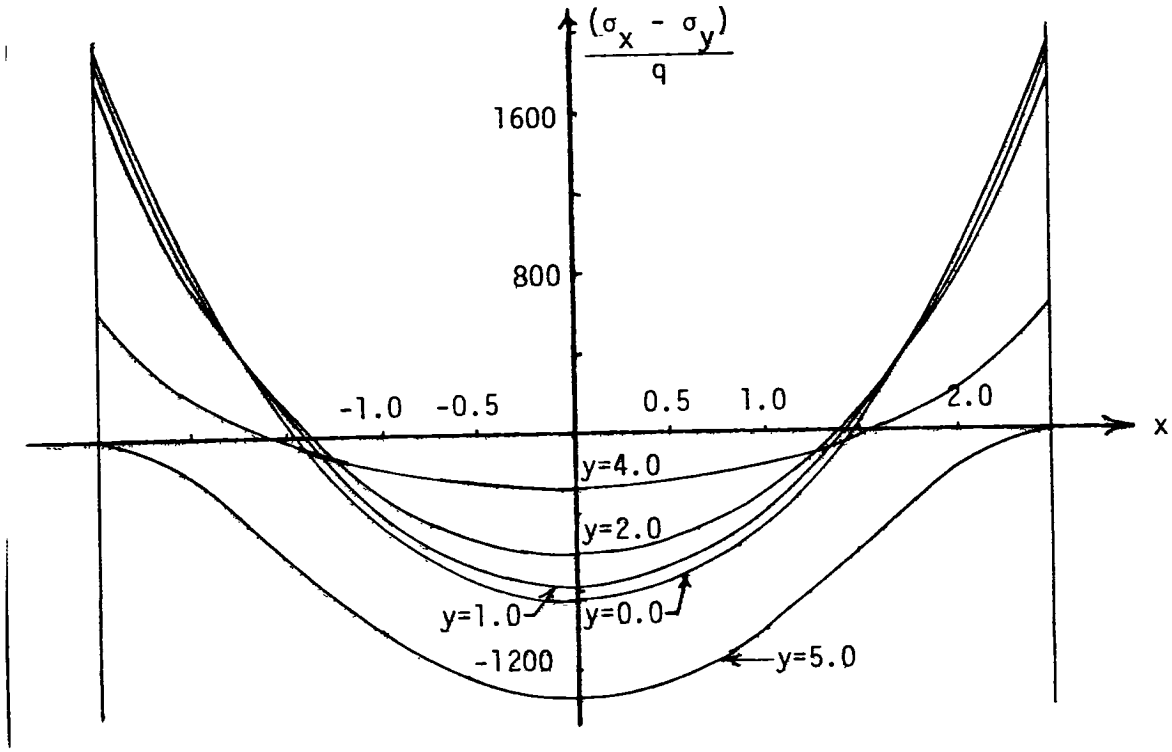

Figure 6. Stress Distribution For
5 mil x 10 mil x 1.69 μm
(1.27×10^{-2} cm x 2.54×10^{-2} cm x 1.69 μm) Diaphragm

To calculate the change in resistance of a finite size resistor due to applied stress, an averaging technique must be applied to convert the point relation $\frac{\Delta\rho}{\rho_o}$ to $\frac{\Delta R}{R_o}$ for the complete resistor. For a p-type diffused resistor whose longitudinal axis lies along the crystals <110> direction, the relationship between the fractional change in resistance and the applied stress can be approximated by Eq. (3), repeated here,

$$\frac{\Delta R}{R_o} = \frac{\pi_{44}}{2} \overline{(\sigma_\ell - \sigma_t)} \tag{9}$$

where $\overline{(\sigma_\ell - \sigma_t)}$ ≡ the difference between longitudinal and transverse stress components average across the entire resistor.

A Wheatstone bridge configuration of resistors on the diaphragm was used instead of a single resistor to increase the output voltages. Making the four resistors of the same size and arranged in a square with the four corners connected facilitates contact to the four resistors and gives the desired orientation of resistors, Fig. 7. The bridge dimensions will then depend on the length of the resistors whose longitudinal axis lie in the x direction (R_x).

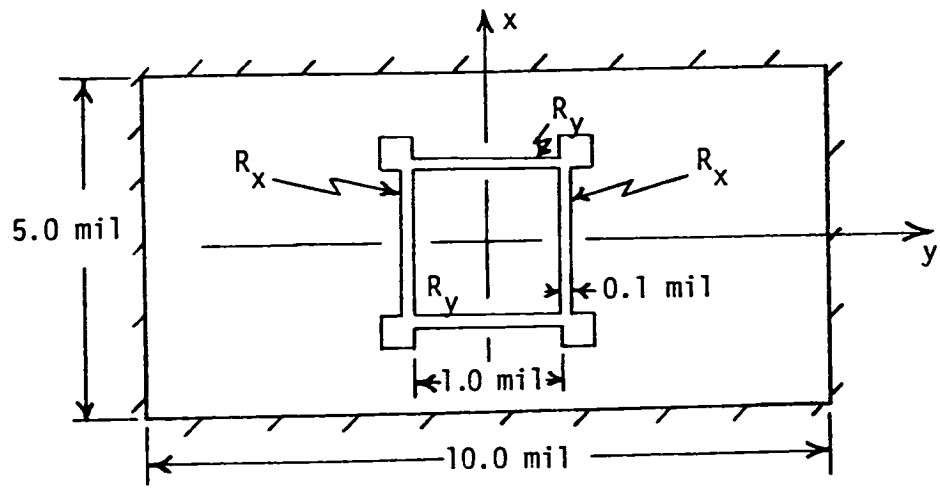

Figure 7. Diffusion Pattern for Piezoresistive Bridge.

For all four resistors an aspect ratio of 10 with a p-diffusion of 100Ω/□ was chosen, giving a stress-free resistance of approximately 1KΩ. The closer the resistors are located to the center, the higher the average magnitude of stress difference, and thus the higher the bridge output. A resistor length of 1 mil was chosen which was about the smallest size considered to be practical for our investigatory studies. The bridge dimensions are shown in Fig. 7.

Once the dimensions and location of the bridge are known, the sensitivity of the bridge can be calculated using the average value of stress for each resistor, Eq. (3), and the equation for the output of a bridge is

$$\left|\frac{V_{out}}{V_{in}}\right| = \frac{\left|\left(\frac{\Delta R}{R_o}\right)_x - \left(\frac{\Delta R}{R_o}\right)_y\right|}{2 + \left(\frac{\Delta R}{R_o}\right)_x + \left(\frac{\Delta R}{R_o}\right)_y} \tag{10}$$

assuming that $\left(\frac{\Delta R}{R_o}\right)_x$ is the same for both R_x resistors and that $-\left(\frac{\Delta R}{R_o}\right)_y$ is the same for both R_y resistors. It can also be assumed that,

$$2 + \left(\frac{\Delta R}{R_o}\right)_x + \left(\frac{\Delta R}{R_o}\right)_y \simeq 2 \tag{11}$$

then (14) becomes

$$\left|\frac{V_{out}}{V_{in}}\right| \simeq \frac{\left|\left(\frac{\Delta R}{R_o}\right)_x - \left(\frac{\Delta R}{R_o}\right)_y\right|}{2} \tag{12}$$

For a 1 MHz pressure sensor whose diaphragm dimensions are 5 mil x 10 mil x 1.69 μm with the bridge pattern shown in Fig. (7), the sensitivity can be calculated with the exact value of the piezoresistance coefficient, π_{44}. The relation between surface concentration and the piezoresistance coefficient has been measured by Tufte and Stelzer [4] for p-type diffused layers having an error function impurity distribution. The results are shown in Fig. (8).

Assuming a p-concentration of about $10^{20}/cm^3$, it gives a value for π_{44} of 70×10^{-12}[cm^2/dyne] = 4.9×10^{-6}/psi. For calculations of the piezoresistance effect, the average stress was estimated from calculations of $(\sigma_x - \sigma_y)$ at 121 equally spaced points covering the entire area of the resistor(s). The average of these values is then taken as $\pm (\sigma_\ell - \sigma_t)$, the $\pm$ depending upon which axis, x(+) and y(-), is parallel to the resistor's longitudinal axis.

If a resistor is positioned such that the magnitude of the stress difference is high in some parts, but low in the remaining area, averaging the stress will decrease the effectiveness of the high stress region. In order to obtain a high piezoresistance effect from the high stress region, the resistor(s) should be confined to these areas and not overlap into areas of low stress. Fig. 4 shows that for a square diaphragm, the resistor would have to be very narrow and positioned very close to the edge of the diaphragm. The magnitude drops from 2608 psi at the edge to 996 psi at 0.5 mil away from the edge. Small resistor and diaphragm sizes and the need for exact positioning of the resistor(s) on the diaphragm necessitate the use of fairly accurate alignment methods and tight restrictions on the diaphragm's dimension to assure the proper location of the resistor in an area of high stress.

As seen before, if the ratio a/b is increased, a region of reasonably high stress difference is apparent in the center of the diaphragm. The stress distribution does not have as high of a slope in this area as it does toward the edges of the diaphragm. Thus even if the magnitude of the stress difference in the center area is not as great as the edge area, its more uniform distribution over a larger area allows for easier positioning of the resistor(s) for a more predictable output for a given input.

Using the previously described averaging technique, the average value of stress difference across the resistors was calculated as

$$\frac{\overline{(\sigma_x - \sigma_y)}}{q} = -790.94 \qquad \text{for } R_x\text{'s}$$

and

$$\frac{\overline{(\sigma_x - \sigma_y)}}{q} = -720.92 \qquad \text{for } R_y\text{'s}$$

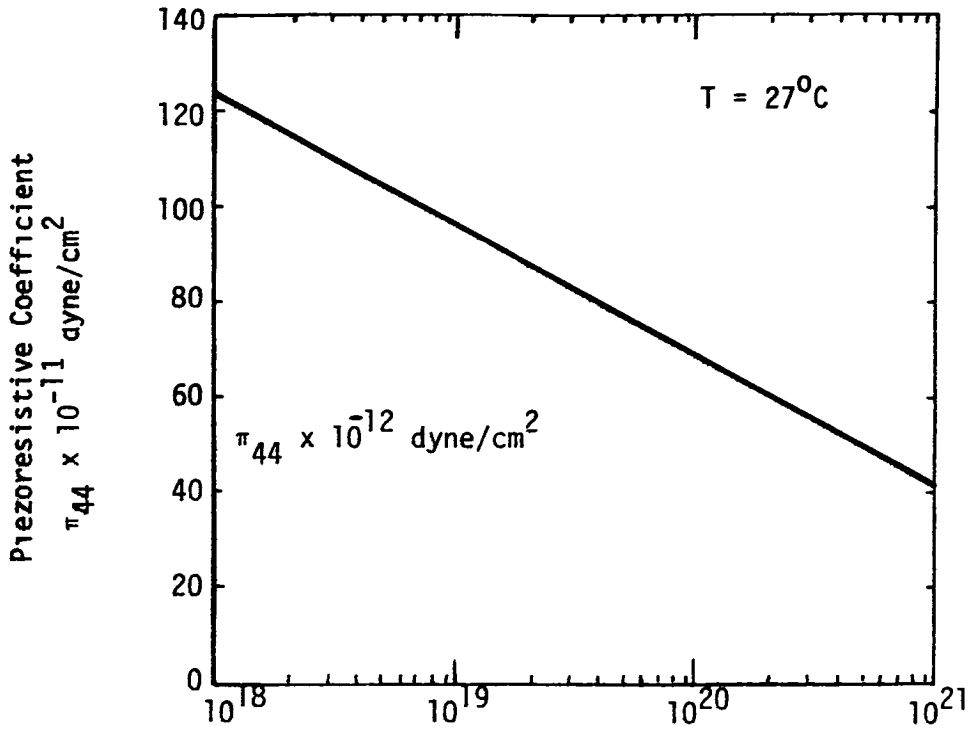

Figure 8: Piezoresistance vs. Surface Concentration of Impurities in Silicon Diffused Layers /cm^3

The above were calculated for a 5 mil x 10 mil x 1.69 μm diaphragm with a pressure of 1 psi applied uniformly to the surface on which the bridge pattern is diffused. The estimated fractional change in resistance for the bridge's legs are,

$$\left(\frac{\Delta R}{R_o}\right)_x = \frac{\pi_{44}}{2}(\sigma_x - \sigma_y)$$

$$= -1.94 \times 10^{-3} \times q \qquad (13\text{-a})$$

$$\left(\frac{\Delta R}{R_o}\right)_y = \frac{-\pi_{44}}{2}(\sigma_x - \sigma_y)$$

$$= 1.77 \times 10^{-3} \times q \qquad (13\text{-b})$$

The calculated sensitivity for the bridge pattern then becomes 1.85 mV/volt input/psi (2.684×10^{-4} mv/v-N/m^2).

FABRICATION AND EXPERIMENTAL WORKS

A. Processing of Silicon Wafers

The following is a brief outline of fabrication procedures. The starting material for the process is (100)-oriented, n-type, 6-8 Ω-cm silicon wafers about 200 μm thick. These wafers have one flat side corresponding to the [110] direction of the silicon crystal. This direction corresponds to the direction of maximum piezoresistance for p-type resistors.

The first step is cleaning of the wafers for 20 minutes in hot ($60^{o}C$) solvent baths (TCE-Trichloroethylene, then acetone) followed by methanol and DI-H_2O rinses. After thorough drying with N_2-gas, the wafer is given a hot acid bath ($70^{o}C$ for 20 minutes, 2 parts H_2SO_4 to 1 part HNO_3). Following the acid bath, wafers should be rinsed with DI-H_2O and dried with N_2 gas. A 1 minute bath in concentrated HF (48%) will remove any oxide which may have formed on the wafer. Follow with a DI-H_2O rinse and N_2-gas dry.

The wafers are then given a thermally grown oxide layer of 10,000 Å. This is done at $1100^{o}C$, 10 minutes dry O_2, 180 minutes open tube steam, then 10 minutes dry O_2 again. This thick oxide layer is required to mask the potassium hydroxide (KOH) anisotropic silicon etchant used in the diaphragm formation.

After coating the wafers with positive photoresist and baking for 30 minutes at $90^{o}C$ (pre-baking), they are exposed to ultraviolet light through the desired mask patterns used for etching the wells for the diaphragm formation. The wafers are developed, rinsed with DIH_2O, dried with N_2-gas and baked for 30 minutes at $120^{o}C$. Touch up paint is then used to cover all but two windows, used to form alignment holes, on opposite sides of the wafer. The reverse side is also completely painted to preserve the SiO_2.

After a bake at 75°C for 30 minutes the wafers are set in a buffered HF solution (etch rate ~ 800Å/min. at 20°C) for about 14 minutes to etch two windows in the SiO_2 for formation of the alignment holes.

The photoresist and paint are then stripped and the wafers are etched using an anisotropic etchant (300 ml DI-H_2O, 300 ml isopropyl-alcohol, and 100 mg. KOH pellets) for 1½ hours at 60°C. This will give a well depth of about 20 μm. The difference in depth between these two wells and the remaining wells will serve as an indicator of the thickness of the diaphragms at the time the alignment holes extend completely through the wafers.

The same photolithography steps are then followed using the same mask. The etched alignment wells should be aligned properly with the windows in the mask. After the buffered HF bath, photoresist and paint stripping, the wafers are etched in the same solution for about 10 hours. It was found that this slower etch rate resulted in smoother, more uniform diaphragm surfaces. The exact etching time is determined by frequently monitoring the diaphragm thickness after the alignment holes etch completely through. The thickness can be estimated with a microscope by finding the difference in the thicknes of the wafer measured through an alignment hole and the depth of a well close to the hole.

After both etchings, the wafers are cleaned very thoroughly using the same procedure employed before the initial oxidation. After the hot acid bath and concentrated HF bath, the wafers are given two different peroxide baths. One bath using NH_4OH and H_2O_2 and the other using HCl and H_2O_2. A BD etchant dip for 10 seconds, DI-H_2O rinse, and drying with N_2-gas complete the cleaning procedure. A layer of thermally grown oxide ~ 3000Å thick is given to each wafer (10 minutes dry O_2, 14 minutes steam, 10 minutes dry O_2 at 1100°C), followed by annealing with N_2-gas for one hour at 1150°C. This oxide layer will be used as a mask during the diffusion step(s).

The standard photolithographic procedure is followed using negative photoresist to open the diffusion pattern windows in the thermally grown SiO_2. The alignment holes are used to assure positioning of the bridge pattern in the center of all the diaphragms. The back side is painted to preserve the oxide layer. After the SiO_2 etching with buffered HF, the wafers are cleaned as before with hot solvents and hot acid (H_2SO_4-HNO_3) baths. From this point they are given the two peroxide baths and dipped in BD etchant, rinsed in DI-H_2O and dried with N_2-gas. They are then diffused immediately to avoid contamination or oxidation from exposure to the atmosphere. Diffusion is done using diborane gas at 1000^oC for p^+ and 900^oC for p diffusion (15 minute deposition, 15 minute drive-in). The piezoresistors, after drive-in, have a surface resistivity of 100 /□. If both p^+ and p diffusion are necessary, the p^+ is done first followed directly by photolithography, cleaning (including peroxide baths), and diffusion for the p-diffused pressure sensing wheatstone bridge.

Following all the necessary diffusions, the wafers are given a chemically vapor deposited (CVD) phosphosilicate glass (PSG) passivation layer of 4000Å. Cleaning with solvents (TCE, acetone, methanol) follows. Photolithography is then done using negative photoresist to open windows in the silox and oxide at the points at which metal contacts are desired. The back side is protected with paint and the wafer then put in siloxide etchant for 10 minutes (etch rate ~ 400Å/minute at 25^oC). If contact to the n-type silicon is desired, an additional photolithographic process must be done to make a window through the thermally grown oxide beneath the passivation layer. Buffered HF, which has a higher etch rate for thermal oxide than siloxide etchant, should be used for this etch.

Resistance measurements were done after the contact windows had been opened to check the previous processing steps. Before metalization, the wafers were dipped in BD etchant (10 seconds) to remove any oxide which

may have formed on the contact windows. The wafers were then coated with a 1 μm layer of aluminum on the diffused side by a vacuum deposition process.

After the aluminum deposition, the usual photolithographic processes were applied to remove the unwanted aluminum with aluminum etchant. An additional step of dicing the wafers into individual chips must be done when a single chip must be mounted to perform certain tests, which will be described in the experimental section.

B. Experimental Work

The experimental work consists of four measurements, the first two measurements were made to verify pressure sensitivity of the sensors. The next experiment is conducted in a shock tube facility to obtain upper limit frequencies of the pressure sensors, and this experiment is followed by the measurement of frequency response in an anechoic chamber.

1. Sensitivity Measurements

The static pressure measurements were initially made to evaluate the pressure sensitivity of the sensors, the differential pressure applied in this measurement is 13.5 psi (9.31×10^4 N/m^2). Also the sensitivity measurement was made with acoustic pressure between 110 and 150 dBs at 1000 Hz, 110 dB acoustic level corresponds to approximately 0.001 psi (6.895) N/m^2).

A typical value of inherent noise levels of the sensors is approximately 2 dBs above the Johnson noise of the silicon sensor and this noise corresponds to approximately 2.5 μv rms output from the silicon sensor. For example the lowest pressure detectable by a 2.5 mv/v-psi (1.723 mv/v-N/m^2) sensitivity sensor is 6.895 N/m^2 (0.001 psi ≈ 110 dB) over 30 KHz bandwidth.

2. Shock Tube Measurements

The upper limit frequencies of the selected pressure sensors were measured in a Shock Tube Facility at NASA-Langley. The upper limit frequency of a sensor was determined from the sensor output voltage profile

corresponding to the initial pressure impulse in the shock tube reaching the sensor. The pressure impulse is known to be 4 psi with a 4 nano-seconds rise-time. The sensor output is displayed on an oscilloscope through an automatic sample and hold equipment.

3. Frequency Response Measurements

The frequency measurements of the sensors were measured in an anechoic chamber, at NASA-Langley, with ¼" OD B & K microphone as a reference. The sensor was aligned at the same horizontal level as the source and positioned in a manner that the normal direction of the pressure sensing diaphragm surface is perpendicular to the acoustic source.

The ranges of frequencies used were from 1 to 16 KHz and from 1 to 40 KHz, these ranges of frequencies were pre-determined by the source characteristics.

C. Experimental Results and Discussion

Experimental results of the silicon pressure sensors fabricated are tabulated in Table III.

Both square and rectangular diaphragm sensors were tested to determine their sensitivities and the first mode natural frequencies. Two sensors with square diaphragms have their pressure sensing square bridge placed off the center of the diaphragm so as to make the sensors pressure sensitive.

The sensors with rectangular diaphragms indicate that the same pressure sensitivity and the first mode natural frequency can be obtained from two sensors with different diaphragm size.

It is found that a sensitivity of approximately 1 mv/v-psi (1.45×10^{-4} m/v-N/m^2) can be obtained with sensor's natural frequency near ½ MHz. Sensors with the larger diaphragm (2.54×10^{-2} cm x 5.08×10^{-2} cm) exhibit lower natural frequencies, and the higher natural frequencies relate to the thicker diaphragm of the sensor.

TABLE III. SENSITIVITY AND NATURAL FREQUENCY

Sensor No.	axb(mils or x 10^{-2} cm)	h(μm)	S(mv/v-psi or x 10^{-4}mv/v-N/m^2)		f(KHz)
063	20x30, 7.62 x 7.62	6.25	1.70	2.47	150
071	25x50, 6.35 x 12.7	8	0.52	0.76	188
035	30x30, 7.62 x 7.62	5	1.80	2.61	120
111	5x10, 1.27 x 2.54	0.85	0.90	1.31	500
131	5x10, 1.27 x 2.54	1.06	0.82	1.20	625
141	10x20, 2.54 x 5.08	2.64	0.60	0.87	390
151	10x20, 2.54 x 5.08	3.04	0.88	1.28	450
161	10x20, 2.54 x 5.08	3.26	0.60	0.87	482

The shock tube test results of sensors #151 and #036 are shown in Figure 9 and 10 respectively. The natural frequencies of these sensors read from the figures indicate 450 KHz and 120 KHz.

Figures 11 and 12 are the typical frequency responses of the silicon pressure sensors tested in an anechoic chamber. Figure 11 represents the frequency response of sensor #035, the deviation in the response is $\pm$ 1.5 dB over the range of 40 KHz. Figure 12 shows $\pm$ 1.0 dB variation over the range of 1 to 16 KHz for sensor #063.

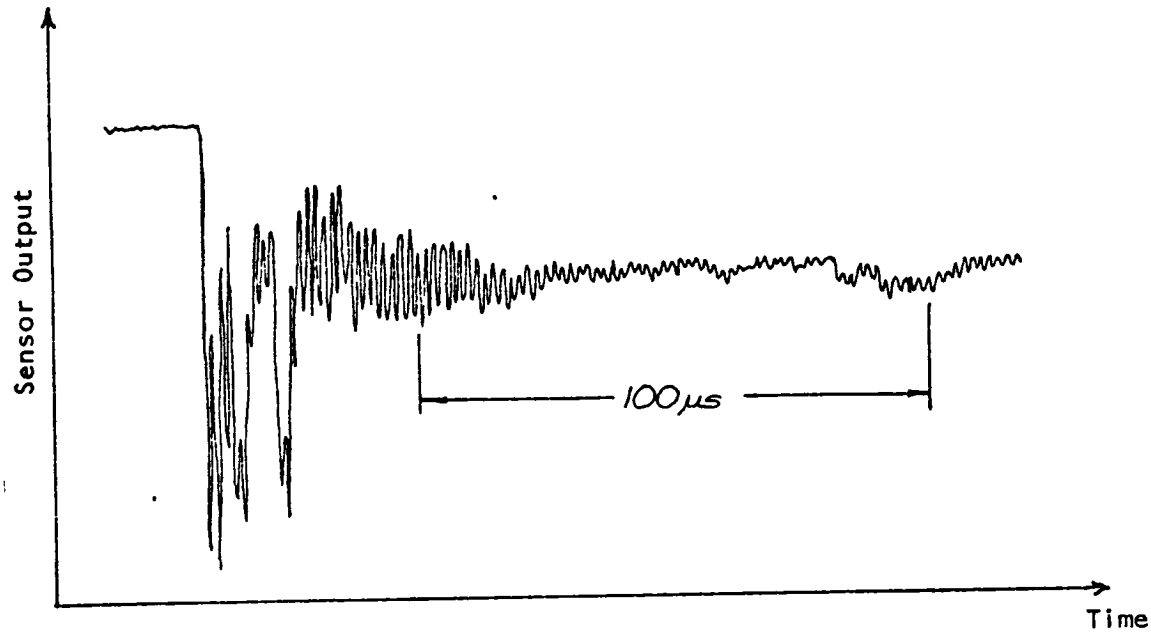

Figure 9. Shock Tube Response, Sensor #151
f_1 = 450 KHz, a x b = 2.54 x 10^{-2} cm x 5.08 x 10^{-2} cm.

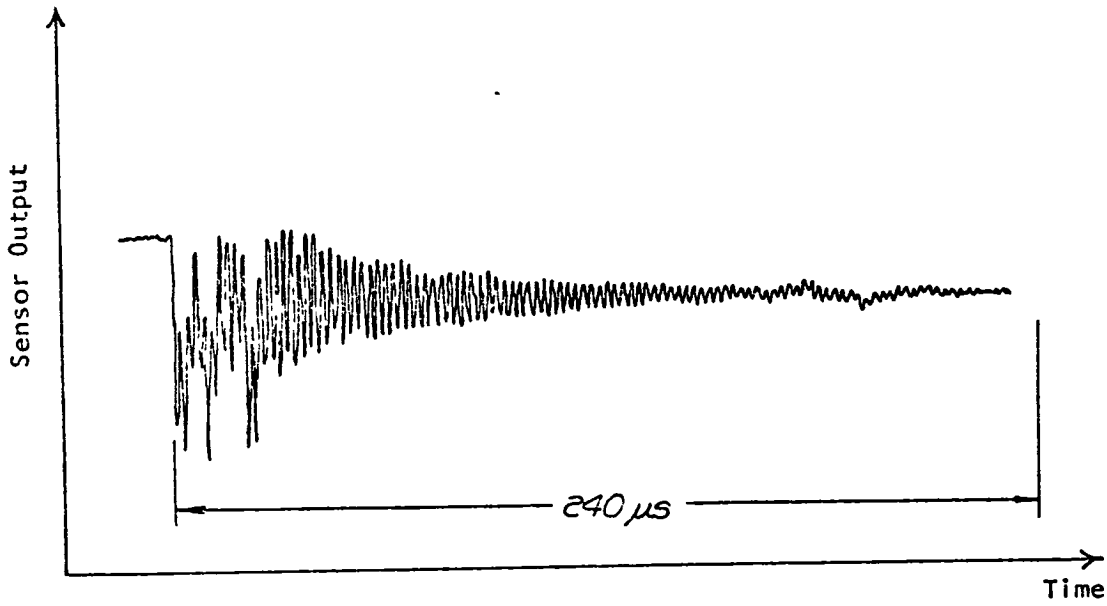

Figure 10. Shock Tube Response, Sensor #151
f_1 = 450 KHz, a x b = 2.54 x 10^{-2} cm x 5.08 x 10^{-2} cm.

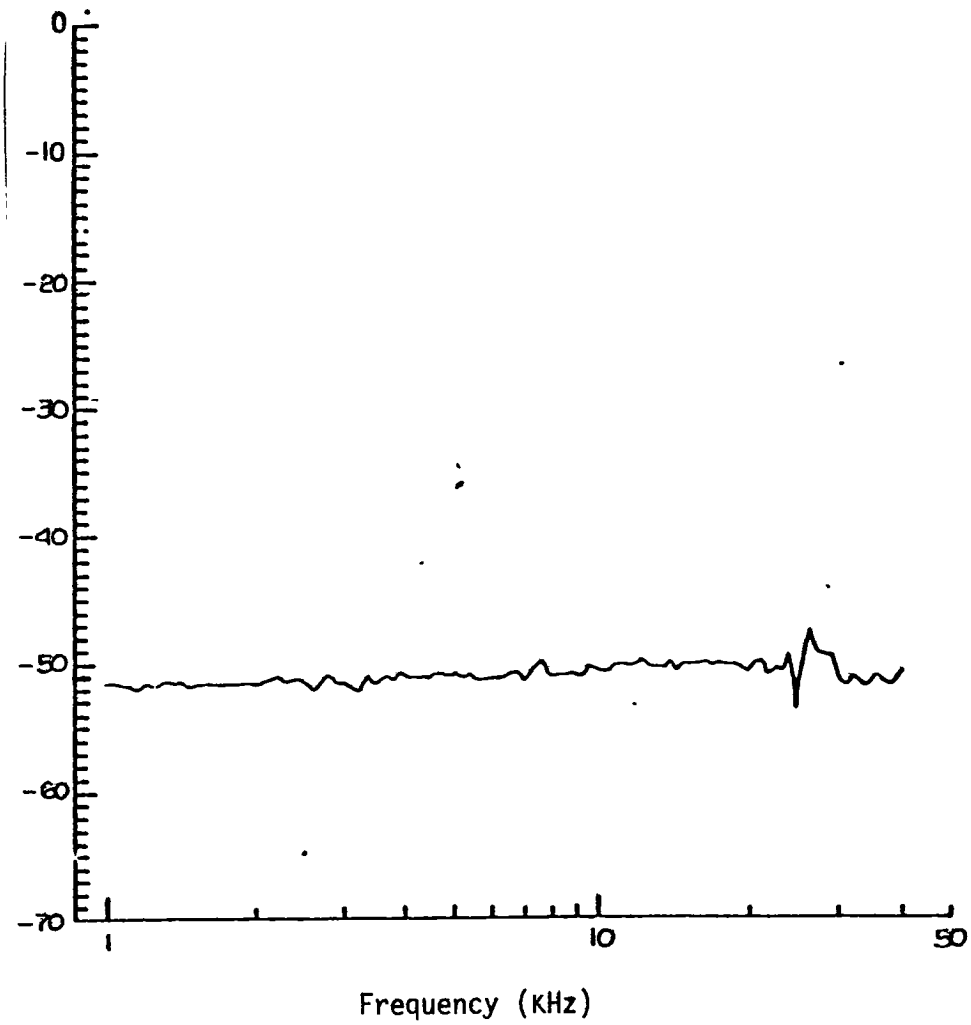

Figure 11. Frequency Response of Sensor #035.

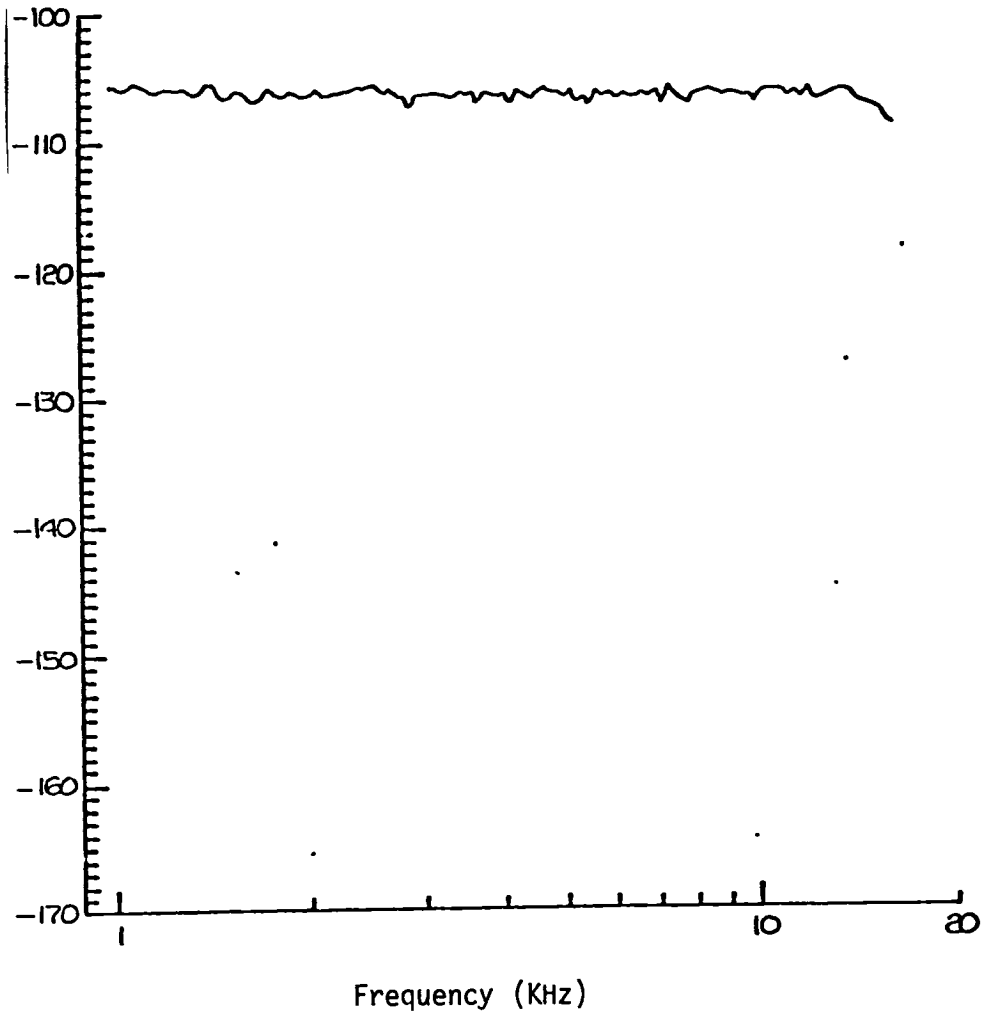

Figure 12. Frequency Response of Sensor #063.

CONCLUSION

The design and fabrication of a small high frequency piezoresistive silicon pressure sensor are presented in this paper. Analysis of stress patterns and vibrational characteristics of the sensor diaphragm are presented. A small transducer is designed with diaphragm dimensions of 1.27×10^{-2} cm x 2.54×10^{-2} cm x 1.06 μm to have a 625 KHz first mode natural frequency, the overall sensor dimensions are 2.54×10^{-1} cm x 3.81×10^{-1} cm x 2.03×10^{-2} cm.

Measurements of the sensor's first mode natural frequency are made with a shock tube test apparatus. The natural frequency of the sensor is found to be 625 KHz, as predicted.

Sensitivity measurements are also made on the transducer. The sensor's performance at both high (9.31×10^{4} N/m^2) and low (6.895 N/m^2) pressure levels indicates a sensitivity of approximately 0.8 mV/V/psi (1.2×10^{-4} mv/v-N/m^2).

Testing of the sensor's frequency response over a continuous range of frequencies is carried out in an anechoic chamber. The sensor's response remains flat within $\pm$ 2.0 dB over the entire range of test frequencies (1-40 KHz).

The tests results demonstrate a silicon piezoresistive pressure sensor can be fabricated to make measurements of high frequency low pressure profiles. The achievable first mode natural frequency and the sensitivity may be 1 MHz and 10^{-4} psi, respectively.

ACKNOWLEDGMENT

The author wishes to acknowledge helpful discussions with John Seiner of NASA-Langley. And Seun K. Kahng wishes to thank Langley Research Center-NASA for their support of this work.

BIBLIOGRAPHY

1. Smith, C.S., "Piezoresistive Effect in Silicon and Germanium," Physical Review, Vol. 94, No. 1, pp. 42-49, January 1954.

2. Samaun et al., "An Integrated Circuit Piezoresistive Pressure Sensor for Biomedical Instrumentation," IEEE Trans. on Biomedical Engineering, Vol. BME-20, No. 2, pp. 101-109, March 1973.

3. Warburton, G.B., "The Vibration of Rectangular Plates," Proceedings of the Institute of Mechanical Engineering, 1953, pp. 371-384.

4. Tufte, O.N., Chapman, P.W., and Long, D., "Silicon Diffused-Element Piezoresistive Diaphragms," Jour. of Applied Physics, Vol. 33, No. 11, pp. 3322-3327, November 1962.

1 Report No	2 Government Accession No	3 Recipient's Catalog No
NASA CR-162752	N80-17424	

4 Title and Subtitle	5 Report Date
MINIATURE PIEZORESISTIVE SOLID STATE INTEGRATED PRESSURE SENSOR	February 1980
	6 Performing Organization Code
7 Author(s)	8 Performing Organization Report No
Seun K. Kahng	
	10 Work Unit No
9 Performing Organization Name and Address	11 Contract or Grant No
University of Oklahoma Norman, Oklahoma 73019	NSG-1481
	13 Type of Report and Period Covered
12 Sponsoring Agency Name and Address	Contractor Report
National Aeronautics and Space Administration Washington, DC 20546	14 Sponsoring Agency Code

15 Supplementary Notes

Contract Monitor: Chris Gross, NASA-Langley Research Center

16 Abstract

The characteristics of silicon pressure sensors with an ultra-small diaphragm are described. The pressure sensors utilize rectangular diaphragms as small as 0.0127 x 0.0254 cm and a p-type Wheatstone bridge consisting of diffused piezoresistive elements, 0.000254 cm by 0.00254 cm. These sensors exhibit as high as 0.5 MHz natural frequency and 1 mV/V/psi pressure sensitivity. Fabrication techniques and high frequency results from shock tube testing and low frequency (< 60 KHz) comparison with microphones are presented.

17 Key Words (Suggested by Author(s))	18 Distribution Statement
Pressure Sensors High Frequency	Star Category 35 Unclassified-Unlimited

19 Security Classif (of this report)	20 Security Classif (of this page)	21 No of Pages	22 Price*
Unclassified	Unclassified	32	

For sale by the National Technical Information Service, Springfield Virginia 22161

End of Document